PHYSICAL REVIEW D **90,** 063007 (2014)

Model-independent fit to Planck and BICEP2 data

Laura Barranco,[1] Lotfi Boubekeur,[1,2] and Olga Mena[1]

[1]*Instituto de Física Corpuscular (IFIC), CSIC-Universitat de Valencia, Apartado de Correos 22085, E-46071, Spain*

[2]*Laboratoire de physique mathematique et subatomique (LPMS) Universite de Constantine I, Constantine 25000, Algeria*

(Received 3 June 2014; published 17 September 2014)

Inflation is the leading theory to describe elegantly the initial conditions that led to structure formation in our Universe. In this paper, we present a novel phenomenological fit to the Planck, WMAP polarization (WP) and the BICEP2 data sets using an alternative parametrization. Instead of starting from inflationary potentials and computing the inflationary observables, we use a phenomenological parametrization due to Mukhanov, describing inflation by an effective equation of state, in terms of the number of e-folds and two phenomenological parameters α and β. Within such a parametrization, which captures the different inflationary models in a model-independent way, the values of the scalar spectral index n_s, its running and the tensor-to-scalar ratio r are *predicted*, given a set of parameters (α, β). We perform a Markov Chain Monte Carlo analysis of these parameters, and we show that the combined analysis of Planck and WP data favors the Starobinsky and Higgs inflation scenarios. Assuming that the BICEP2 signal is not entirely due to foregrounds, the addition of this last data set prefers instead the ϕ^2 chaotic models. The constraint we get from Planck and WP data alone on the *derived* tensor-to-scalar ratio is $r < 0.18$ at 95% C.L., value which is consistent with the one quoted from the BICEP2 Collaboration analysis, $r = 0.16^{+0-06}_{-0.05}$, after foreground subtraction. This is not necessarily at odds with the 2σ tension found between Planck and BICEP2 measurements when analyzing data in terms of the usual n_s and r parameters, given that the parametrization used here, for the preferred value $n_s \simeq 0.96$, allows only for a restricted parameter space in the usual (n_s, r) plane.

DOI: 10.1103/PhysRevD.90.063007 PACS numbers: 98.70.Vc, 98.80.Cq, 98.80.Bp

I. INTRODUCTION

The recent claimed discovery of primordial B-modes by the BICEP2 Collaboration [1,2] has spurred a lot of interest in the cosmology community. One of the main topics of discussion is the tension between the BICEP2 results and the previous ones. In particular, this measurement corresponds to a tensor-to-scalar ratio of[1] $r = 0.2^{+0.07}_{-0.05}$, while the Planck TT data [combined with WMAP polarization (WP) data, high-ℓ CMB measurements and without running of the scalar spectral index] [3,4] gives $r < 0.11$ at 95% C.L. As argued in [1], allowing for a running of the scalar spectral index makes the two data sets compatible at the 1σ level. On the other hand, the large-field slow-roll models are able to explain successfully the BICEP2 data, however they predict negligible running, which, indeed, has not been seen in any previous observation like e.g. Planck. This by itself suggests a nontrivial departure from the simple single-field slow-roll inflation paradigm. Plenty of effort has been devoted in the literature to reconcile BICEP2 and Planck observations, either by modifications of the inflationary sector [5–11] and/or of the standard cosmological scenario, as, for instance, extensions to the neutrino sector [12–17]. Implications of the BICEP2 results in terms of the usual inflationary parameters have also been extensively explored [18–20]. In this work, we will look at this issue with a different perspective; we shall use an alternative parametrization to fit both Planck and BICEP2 observations. There are two aspects of this discrepancy that are worth pursuing. The first one is purely experimental/observational and implies a reassessing of all the systematic errors and possible unaccounted-for foregrounds (see [21] for a recent analysis in this direction). Despite the tremendous and impressive work done by the BICEP2 Collaboration, this step is mandatory before drawing any definitive conclusion about the cosmological origin of this signal. For a road map of this program, see e.g. [22]. In the following, we will be assuming that the BICEP2 signal is primordial, although the novel phenomenological approach presented here can be applied to fit any cosmological data. The second aspect is theoretical, and it addresses the crucial question: Did our Universe suffer a quasi–de Sitter expansion phase driven by the potential energy of a scalar field (the inflaton)? If yes, then, among the variety of available inflationary scenarios, which one describes better the observations? And, what are the physical implications of such a scenario? In treating this last question, it is customary to use single-field slow-roll models as benchmark scenarios against which the

[1]This figure is obtained without subtracting polarized dust foregrounds, though the signal seen by BICEP2 outweighs any known foreground. Using the best available foreground template shifts the measured value to $r = 0.16^{+0.06}_{-0.05}$.

temperature anisotropies observational data are tested. This is justified by the simplicity of these models when it comes to computing their predictions. Given a simple potential $V(\phi)$, where ϕ is the canonically normalized inflaton field, one can compute easily the observational predictions in terms of the slow-roll parameters ϵ and η defined as[2]

$$\epsilon \equiv \frac{1}{2} M_P^2 (V'/V)^2 \quad \text{and} \quad \eta \equiv M_P^2 V''/V, \tag{1}$$

where the primes denote derivatives with respect to ϕ, i.e. $V' \equiv dV/d\phi$ and so on. During slow-roll, these parameters are small i.e. ϵ, $|\eta| \ll 1$, and the energy density of the Universe is given approximately by the potential $V \simeq 3M_P^2 H^2$, where H is the Hubble expansion rate during inflation. At leading order in slow-roll, the basic observables—the tensor-to-scalar ratio r and the spectral index n_s—are given by

$$r = 16\epsilon_* \quad \text{and} \quad n_s = 1 + 2\eta_* - 6\epsilon_*, \tag{2}$$

where the subscript $*$ is to remind that quantities are evaluated at horizon exit. These quantities are usually the basic ones used when testing models against observations. Each potential $V(\phi)$ corresponds to a certain set of observables (r, n_s), but in general, these parameters are expected to be $O(1/N_*)$ where N_* is the number of e-folds starting from horizon exit, necessary to solve the standard cosmological problems. In general, this number has a mild dependence on the cosmological history, however under rather reasonable assumptions, N_* takes values in the range $N_* \simeq 50$–60, that we adopt from now on in our analysis.

Instead of the usual slow-roll parametrization, one can use a more phenomenological and intuitive way of describing the inflationary phase through its equation of state [25]. During inflation, the equation of state is $p \simeq -\rho \simeq -3H^2 M_P^2$, up to slow-roll corrections, while at the end of inflation $\dot{\phi}^2/2 \simeq V(\phi) \simeq \rho/2$ and the equation of state is instead $p \simeq 0$. One can thus write that

$$\frac{p}{\rho} = -1 + \frac{\beta}{(1+N_e)^\alpha}, \tag{3}$$

where α and β are phenomenological parameters and are both positive and of $O(1)$, and N_e is the number of remaining e-folds to end inflation $N_e(t) \equiv \int_t^{t_e} dtH$ and it runs from N_*, at horizon exit, to 0, when inflation ends. Using energy conservation $\dot{\rho} + 3H(\rho + p) = 0$ one gets the following expressions for the tilt and tensor fraction [25]:

$$n_s - 1 = -3\frac{\beta}{(N_*+1)^\alpha} - \frac{\alpha}{N_*+1}, \tag{4a}$$

$$r = \frac{24\beta}{(N_*+1)^\alpha}. \tag{4b}$$

The general prediction of the ansatz Eq. (3) is that the tilt is always *negative*, irrespective of the inflationary scenario. In contrast, the value of the tensor-to-scalar ratio can take any value depending on both α and β. In addition, one can compute the running of the tilt

$$\alpha_s \equiv dn_s/d\log k = -\frac{3\alpha\beta}{(1+N_*)^{\alpha+1}} - \frac{\alpha}{(N_*+1)^2}, \tag{5}$$

which is, like the tilt, always *negative*.

The parametrization Eq. (3) encodes a variety of models with completely different predictions [25]. Notice however that this phenomenological description of the inflationary phase is not completely equivalent to the slow-roll picture, as there is no more freedom in the signs of both the tilt and the running.

From Fig. 1, it is clear that the observationally preferred value of the scalar spectral index $n_s \simeq 0.96$ corresponds to two different branches. The first one lies close to the horizontal line $r \approx 0$, in Fig. 1, and contains for instance Starobinsky models of inflation [24], which are based on the Lagrangian $\sqrt{-g}(R + aR^2)$. In terms of the phenomenological parametrization Eq. (3), this branch corresponds

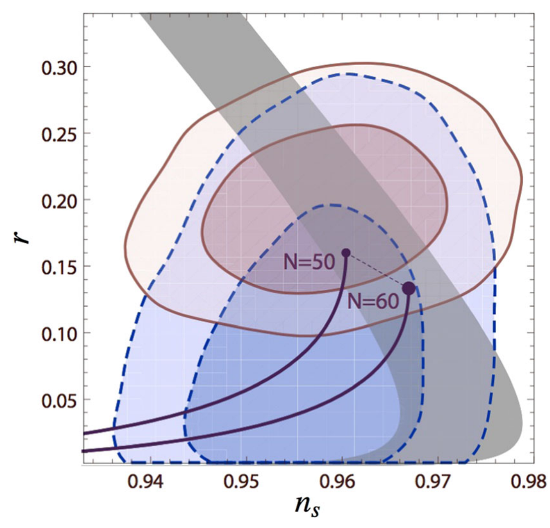

FIG. 1 (color online). Confidence regions in the (n_s, r) parametrization plane. The blue (dashed boundary) areas represent the 68% and 95% C.L. regions of Planck (including a nonzero running), while the red (solid boundary) areas are the 68% and 95% C.L. regions for BICEP2 only. The gray band represents the predictions of the models captured by the parametrization Eq. (3) for $50 \le N_* \le 60$. The solid magenta lines correspond to the natural inflation scenario. For large decay constant $f \gg M_P$, they reduce to the $V \propto \phi^2$ scenario (short-dashed magenta line).

[2]For a nice review of slow-roll inflation see e.g. [23]. Throughout the paper, we will adopt natural units $\hbar = c = 1$. As usual, the reduced Planck scale is given by $M_P = (8\pi G_N)^{-1/2} \simeq 2.43 \times 10^{18}$ GeV.

to $\alpha = 2$, and $r \simeq 10^{-2}\beta$. In particular [25], Starobinsky inflation corresponds to $\beta = 1/2$.

In contrast, the second branch, with significantly higher tensor fraction (appearing as a thick diagonal gray area in Fig. 1) is where chaotic inflation models $V(\phi) \propto \phi^n$ [26] live. In terms of the parametrization Eq. (3), chaotic scenarios live on the line corresponding to $\alpha = 1$. From Eqs. (4), the line in the (n_s, r) plane is given by $n_s \simeq 1 - \frac{r}{8}$, up to an $O(1/N_*)$ correction. On the other hand, the parameter β fixes the power of the potential $V \propto \phi^n$, as $n = 6\beta$.

The natural inflation scenario [27,28], in which the inflaton is a pseudo-Nambu-Goldstone boson, is represented by the purple line in Fig. 1. This scenario described by the potential $V(\phi) \propto [1 - \cos(\phi/f)]$ is captured by the parametrization Eq. (3) but only for large enough decay constants $f \gtrsim 10M_P$. We recall that in the limit of very large decay constant, $f \gg M_P$, Natural inflation reduces to the ϕ^2 scenario represented by the thick purple dots ($N_* = 50$ and $N_* = 60$) in Fig. 1.

Before describing our cosmological data fits, let us determine the interval spanned by the phenomenological parameters α and β. First, as explained in Ref. [25], given that inflation ends, i.e. $N_e \to 0$, when $p/\rho \approx 0$, it follows that β cannot be much larger that 1. Second, given that in the most optimistic situation, the tensor-to-scalar ratio will be measured at an accuracy of [22] $\Delta r/r = 10^{-2}$, it is clear from Eq. (4b) that[3] $\alpha \lesssim 2.5$. We shall adopt these priors in our numerical analyses.

The structure of the paper is as follows. In Sec. II, we describe the method followed when performing the fits to the different data sets. Next, in Sec. III, we present our results in terms of the parameters α and β governing the parametrization Eq. (3), and in terms of the *derived*, most commonly used inflationary parameters n_s and r. We also discuss their implications. Finally, we draw our conclusions in Sec. IV.

II. DATA ANALYSIS

A. Method

The phenomenological scenario we explore is described by the following parameter set:

$$\{\omega_b, \omega_c, \Theta_s, \tau, \log[10^{10}A_s], \alpha, \beta\}, \quad (6)$$

[3] A meaningful measurement of the tensor-to-scalar ratio implies that $\Delta r \lesssim r$. Using Eq. (4b), one gets

$$\alpha \lesssim \log(24\beta/\Delta r)/\log(N_* + 1),$$

which for $\beta \lesssim 1$ and the optimistic percent-level observational error on $r \simeq 0.001$ targeted e.g. by COrE [29] and PIXIE [30] gives $\alpha \lesssim 2.5$. Notice that the above estimate does not change appreciably as it depends only logarithmically on both N_* and Δr.

TABLE I. Uniform priors for the cosmological parameters considered here.

Parameter	Prior
$\Omega_b h^2$	$0.005 \to 0.1$
$\Omega_c h^2$	$0.001 \to 0.99$
Θ_s	$0.5 \to 10$
τ	$0.01 \to 0.8$
$\log(10^{10}A_s)$	$2.7 \to 4$
α	$0 \to 2.5$
β	$0 \to 1$

where $\omega_b \equiv \Omega_b h^2$ and $\omega_c \equiv \Omega_c h^2$ are the physical baryon and cold dark matter energy densities, Θ_s is the ratio between the sound horizon and the angular diameter distance at decoupling, τ is the reionization optical depth, A_s the amplitude of the primordial spectrum and α and β are the phenomenological parameters governing the parametrization given in Eq. (3). In the following, we fix the number of e-folds to $N_* = 60$. Furthermore, we assume that dark energy is described by a cosmological constant. Table I specifies the priors considered on the cosmological parameters listed above. The commonly used (n_s, r) parameters can be easily obtained using Eqs. (4), however unlike the usual case where the running of the spectral index is a free parameter, the running here is completely fixed through Eq. (5), given (α, β) and N_*. In our analysis, we also consider the so-called inflation consistency relation relating the tensor spectral index to r through $n_T = -r/8$, which is also valid in this parametrization.[4] For our numerical calculations, we use the CAMB Boltzmann code [32] deriving posterior distributions for the cosmological parameters from the data sets described in the next section by means of Markov Chain Monte Carlo (MCMC) analyses. Our MCMC results rely on the publicly available MCMC package COSMOMC [33] that implements the Metropolis-Hastings algorithm.

B. Cosmological data

In our analyses we will consider, as a basic data set: the Planck CMB temperature anisotropies data [34,35] together with the nine-year polarization data from the WMAP satellite [36]. The total likelihood for the former data is obtained by means of the Planck Collaboration publicly available likelihood code, see Ref. [35] for details. The Planck temperature power spectra extend up to a maximum multipole number $\ell_{\max} = 2500$, while the nine-year WP polarization data are analyzed up to a maximum multipole $\ell = 23$ [36].

As stated before, very recently, the BICEP2 Collaboration has found evidence for the detection of B-modes in the multipole range $30 < \ell < 150$ spanned by

[4] See Eq. (8.125) of [31].

their three-year data set [1,2], with 6σ significance. The detected B-mode signal exceeds any known systematics and/or expected foregrounds and is well fitted with a tensor-to-scalar ratio $r = 0.2^{+0.07}_{-0.05}$. The BICEP2 likelihood has been properly accounted for in our MCMC numerical analyses, by using the latest version of COSMOMC.

III. RESULTS

We represent the results of our MCMC analyses both in the (α, β) plane and in the usual (n_s, r) plane. Figure 2 shows the 68% and 95% C.L. contours in (α, β). The red solid contours depict the 68% and 95% C.L. allowed regions from the combined analysis of Planck, WP and BICEP2 data, while the blue dashed contours refer to the 68% and 95% C.L. allowed regions from the analysis of Planck and WP data. The green dotted region represents the limits in the (α, β) plane inferred from the 1σ preferred values for n_s and r from Planck and BICEP2 data, respectively. Notice that the results from our MCMC analyses after the combination of Planck, WP and BICEP2 data sets lie precisely within this region. The combination of Planck and WP data is completely insensitive to the β parameter, as β sets the amount of gravitational waves. The addition of BICEP2 data, however, strongly constrains the value of β, as illustrated in Fig. 3, which shows the one-dimensional probability density for the β parameter before and after the inclusion of BICEP2 measurements. Figure 3 shows as well the best fit and the 1σ allowed regions for the β parameter after considering all the measurements exploited in this study. We also depict in Fig. 3 the value of β for the most favored inflationary scenario, as we shall see in what follows.

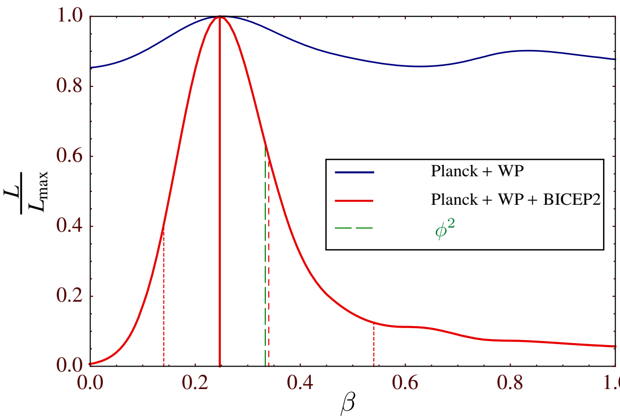

FIG. 3 (color online). The derived likelihood distribution for the phenomenological parameter β of Eq. (3) using different data sets. The red thick (solid and dashed) vertical lines represent the best fit ($\pm 1\sigma$ intervals) of β, while the red thin-dashed line stands for the derived mean value of β, see Table II for details. The quadratic chaotic scenario, corresponding to $\beta = 1/3$, is represented by a green long-dashed line.

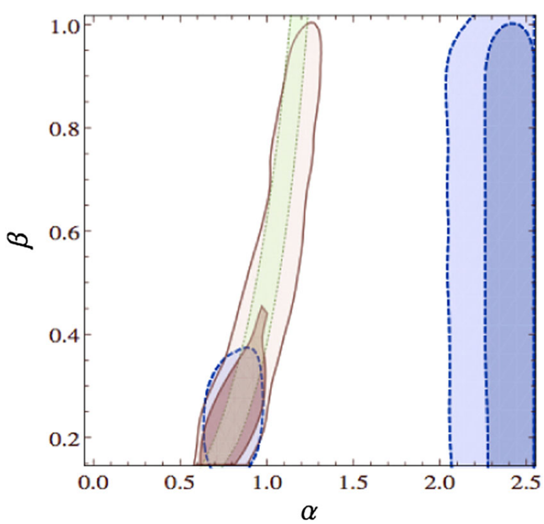

FIG. 2 (color online). Confidence regions in the (α, β) parameters in Eq. (3). The red areas (solid boundary) represent the 68% and 95% C.L. allowed regions arising from a combined analysis of the Planck, WP and BICEP2 data, while the blue areas (dashed boundary) are the 68% and 95% C.L. allowed regions from the analysis of Planck and WP data. The green region with dotted contours represents the joint 1σ preferred region for Planck and BICEP2.

Figure 4 depicts the 68% and 95% C.L. allowed contours in the plane of the *derived* parameters n_s and r, together with the region covered by the parametrization given by Eq. (3) for $50 \leq N_* \leq 60$. Table II shows the constraints at 68% confidence level on the cosmological parameters considered in our MCMC analyses for the different data combinations explored here. Notice that, when BICEP2 measurements are not considered, $\alpha = 2.24 \pm 0.43$ while $\beta = 0.50 \pm 0.28$, which corresponds to $n_s \simeq 0.96$

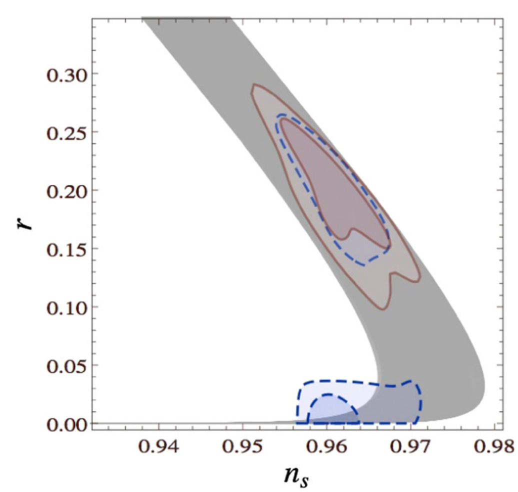

FIG. 4 (color online). Confidence regions of the *derived* parameters (n_s, r) using the parametrization given by Eq. (3). The color coding is the same as in Fig. 1. The gray band represents the predictions of the models covered by the parametrization given by Eq. (3) for $50 \leq N_* \leq 60$.

TABLE II. Constraints at 68% confidence level on cosmological parameters from our analyses for Planck + WP and Planck + WP + BICEP2 data. When quoting upper bounds, we show the 95% C.L. limits. Notice that the scalar spectral index and the tensor-to-scalar ratio are *derived* parameters.

Parameter	Planck + WP	Planck + WP + BICEP2
$\Omega_b h^2$	0.0209 ± 0.0002	0.0209 ± 0.0002
$\Omega_c h^2$	0.1165 ± 0.0018	0.1167 ± 0.0020
θ	1.0409 ± 0.00055	1.0408 ± 0.00055
τ	0.086 ± 0.015	0.078 ± 0.013
$\log[10^{10} A_s]$	3.063 ± 0.031	3.047 ± 0.026
α	2.24 ± 0.43	0.88 ± 0.17
β	0.50 ± 0.28	0.34 ± 0.20
n_s *(derived)*	0.961 ± 0.002	0.961 ± 0.003
r *(derived)*	< 0.18	0.195 ± 0.037

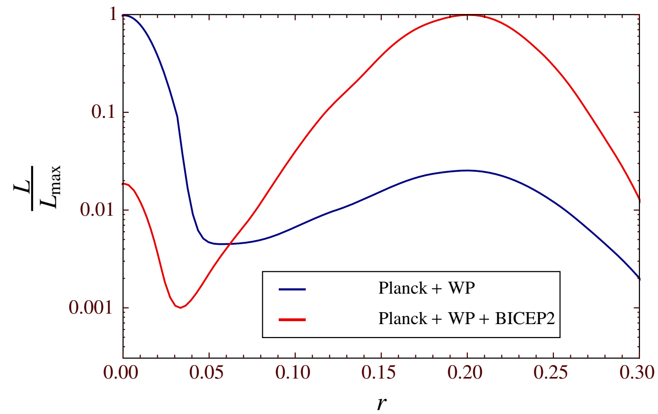

FIG. 5 (color online). The derived posterior likelihood distribution for the tensor-to-scalar ratio using different data sets.

and $r < 0.18$ at 95% C.L., values that can clearly be inferred from the results depicted in Fig. 4. The constraint we get for Planck and WP data alone is $r < 0.18$ at 95% C.L., value to be compared with the value quoted for BICEP2 Collaboration for $r = 0.16^{+0.06}_{-0.05}$ [1] after subtracting the various foregrounds. Therefore, the upper limits we get on the tensor-to-scalar ratio r from Planck and WP data using the parametrization given in Eq. (3) are very close to the figure of $r = 0.16^{+0.06}_{-0.05}$ reported by the BICEP2 Collaboration. This is consistent with the tension found between BICEP2 and Planck using the standard parameters n_s and r, as the parametrization used here includes implicitly a nonvanishing running spectral index, see Eq. (5).

The resulting favored values of $n_s \simeq 0.96$ and $r \approx 0$ from the Planck and WP data analysis may be associated to the Starobinsky model of inflation [24]. Indeed, in terms of the phenomenological parametrization Eq. (3), Starobinsky inflation corresponds to $\alpha = 2$ and $\beta = 1/2$ [25]. Another inflationary scenario that can also be identified with these values of α and β is Higgs inflation, in which the Standard Model Higgs boson itself is responsible for inflation [37,38]. Higgs inflation predicts a scalar spectral index $n_s \simeq 0.97$ and a tensor-to-scalar ratio $r \simeq 0.0033$ for $N_* = 60$ [37] and is indistinguishable observationally from the Starobinsky model.

We can learn from the red contours in Figs. 2 and 4 that, when adding to Planck and WP data the BICEP2 measurements, models with such large values of $\alpha \sim 2$ are no longer favored. The resulting mean values of the two parameters are $\alpha = 0.88 \pm 0.17$ and $\beta = 0.34 \pm 0.20$, which correspond to $n_s = 0.961 \pm 0.003$ and $r = 0.195 \pm 0.037$ (see Table II). This value of r belongs to the second of the branches associated to $n_s \simeq 0.96$, which are depicted by the thick diagonal gray area in Figs. 1 and 4. The one-dimensional posterior probability densities for the *derived* scalar-to-tensor ratio r are depicted in Fig. 5. Notice that for the two possible data combinations the probability distribution is bimodal, showing two maxima: one is located at $r \simeq 0$ and the other one is located at $r \simeq 0.2$. These two peaks stand for the two possible values of r corresponding to $n_s \simeq 0.96$. Each of them is located in one of the two branches shown in Figs. 1 and 4. While the probability distribution function for Planck + WP data has a global maximum at the $r \simeq 0$ branch, the addition of BICEP2 measurements displaces the global maximum towards the $r \simeq 0.2$ region in the other possible branch. As explained before, it is precisely in this second branch where chaotic inflation models $V(\phi) \propto \phi^n$ live [25]. Chaotic models with quadratic (quartic) potentials predict $n_s \simeq 0.96$ and $r \simeq 0.16$ ($n_s \simeq 0.94$ and $r \simeq 0.32$) [25]. Therefore, the mean values of α and β resulting from the combined analyses of Planck, WP and BICEP2 data seem to favor ϕ^2 models of chaotic inflation and highly disfavor Starobinsky and Higgs inflation scenarios. The quartic chaotic model also is disfavored with respect to the quadratic one. The status of the former two inflationary models has also been explored recently in the literature (see e.g. Refs. [39–41]) where it has been found that these two models require either extreme fine-tuning or nontrivial extensions to be compatible with BICEP2 results. Chaotic inflationary models have also been recently revisited in a number of analyses [42–48]. On the other hand, Natural inflation is the only case which cannot be analyzed in terms of α and β except in the large decay constant regime i.e. $f \gg M_P$, where M_P is the Planck mass. In this case, the constraints are similar to the case of the quadratic chaotic scenario (see Fig. 1). Our derived bound on the tensor-to-scalar ratio ($r < 0.18$ at 95% C.L.) does not put significant constraints on f. If on the other hand, we include the BICEP2 data sets, we can translate the 1σ interval into a lower bound on the decay constant $f \gtrsim 44.72 M_P$ for $N_* = 50$. This makes Natural inflation practically indistinguishable from the quadratic chaotic scenario, given the present precision. The next generation of observations will improve the situation considerably, allowing for instance to distinguish between the two scenarios if $f \lesssim 30 M_P$.

See e.g. Refs. [42,49,50] for recent appraisals of the Natural inflation scenario. The results previously discussed have been obtained fixing the number of e-folds to $N_* = 60$. Assuming $N_* = 50$ instead does not change the main conclusions outlined above.

We conclude this section commenting on the results obtained when using a slightly different upper prior on the α parameter. In general, smaller values of α will give rise to a higher tensor-to-scalar ratio and therefore the tension between Planck and BICEP2 measurements may be alleviated. If we assume an upper prior on α of 2, the 95% C.L. upper bound on the derived tensor-to-scalar ratio parameter is slightly larger ($r < 0.23$ at 95% C.L.). On the contrary, when higher values for α are considered, the significance of the tension between Planck and BICEP2 measurements slightly increases, as higher values of α correspond to lower values of r. A fit to Planck and WP data gives an upper limit on $r < 0.17$ at 95% C.L. when using an upper prior on α of 3. When BICEP2 measurements are included in the analysis, we obtain $n_s = 0.961 \pm 0.004$ and $r = 0.184 \pm 0.040$ ($n_s = 0.961 \pm 0.004$ and $r = 0.192 \pm 0.037$) for an upper prior on α of 2 (3). These results are almost identical to the ones quoted in Table II. We have also checked that the posterior probability density profiles for both the parameter β and the tensor-to-scalar ratio r do not exhibit a significant prior dependence. Summarizing, the effect of the upper prior choice on α barely changes our main results.

IV. CONCLUSIONS

The recent claimed discovery of primordial gravitational waves by the BICEP2 Collaboration has opened a new window into the inflationary paradigm. Chaotic inflation scenarios, highly disfavored by Planck temperature data, are, after BICEP2 results, among the most plausible ones. Model-independent data analyses are usually presented in terms of the scalar spectral index n_s and the tensor-to-scalar ratio r, which can then be related to a particular model via the inflationary slow-roll parameters. Here we employ an alternative parametrization due to Mukhanov, describing inflation by an effective equation of state, which captures most of the relevant inflationary scenarios (at least in their basic formulation). Using this parametrization, one can easily identify the different models as well as *derive* the usual n_s and r parameters. The effective equation of state used here is described by only two parameters, α and β, since the running of the spectral index α_s is no longer a free parameter, as is unambiguously determined once the values of α and β are fixed.

Using Markov Chain Monte Carlo methods, we show that the combined analyses of Planck temperature and WP data are unable to determine β, as this last parameter sets the amount of gravitational waves through Eq. (4b). However, these two data sets are able to constrain the other parameter involved, α, resulting in a mean value $\alpha = 2.24 \pm 0.43$, which corresponds to $n_s \simeq 0.96$. Such value of α favored by the Planck and WP data analyses is associated to both Starobinsky and Higgs inflationary models. The constraint we get on the *derived* tensor-to-scalar ratio, $r < 0.18$ at 95% C.L., is perfectly consistent with the value quoted from the BICEP2 Collaboration ($r = 0.16^{+0.06}_{-0.05}$ [1]) after subtracting the various foregrounds. However, this is not necessarily in conflict with the 2σ tension found between Planck and BICEP2 measurements when analyzing data in terms of the usual n_s and r parameters, since the parametrization used here only covers a certain region in the usual plane, see Fig. 1, where it can be noticed that for $n_s \simeq 0.96$ (which is the mean value arising from our numerical analyses) there are only two isolated regions, one at $r \simeq 0$ and second one at $r \simeq 0.2$. Consequently, the likelihood distribution for r is bimodal, and not a monotonically decreasing function with only one maximum located at $r \simeq 0$, weakening the 95% C.L. upper limit on r.

The addition of BICEP2 data to Planck and WP measurements strongly constrains the values of the phenomenological parameters to the values $\beta \simeq 1/3$, and $\alpha \simeq 1$. Such values of α correspond to chaotic inflationary models characterized by a potential ϕ^n, where $n = 6\beta$. Therefore, the results from the combined analysis of Planck, WP and BICEP2 data strongly favor ϕ^2 models of chaotic inflation and rule out Starobinsky and Higgs inflation scenarios. Upcoming polarization data from Planck may confirm or falsify the ϕ^2 scenario as the most plausible one for the inflationary period. Future CMB missions, such as COrE [29] and PIXIE [30], combined with galaxy clustering and weak lensing data from the Euclid survey [51] hold the key to establish the amount of primordial B-modes and the ensuing theoretical implications, especially if the tensor-to-scalar ratio is as large as suggested by BICEP2.

ACKNOWLEDGMENTS

We are grateful to Paolo Creminelli, Scott Dodelson, Carlos Peña Garay and Aaron C. Vincent for their invaluable comments and suggestions on this work. O. M. is supported by the Consolider Ingenio Project No. CSD2007-00060, by PROMETEO/2009/116, by the Spanish Ministry Science Project No. FPA2011-29678 and by the ITN Invisibles PITN-GA-2011-289442.

[1] P. A. R. Ade *et al.* (BICEP2 Collaboration), Phys. Rev. Lett. **112**, 241101 (2014).
[2] P. A. R. Ade *et al.* (BICEP2 Collaboration), Astrophys. J. **792**, 62 (2014).
[3] P. A. R. Ade *et al.* (Planck Collaboration), arXiv:1303.5076 [Astron. Astrophys. (to be published)].
[4] P. A. R. Ade *et al.* (Planck Collaboration), arXiv:1303.5082.
[5] C. R. Contaldi, M. Peloso, and L. Sorbo, J. Cosmol. Astropart. Phys. 07 (2014) 014.
[6] V. Miranda, W. Hu, and P. Adshead, Phys. Rev. D **89**, 101302 (2014).
[7] M. Kawasaki and S. Yokoyama, J. Cosmol. Astropart. Phys. 05 (2014) 046.
[8] K. N. Abazajian, G. Aslanyan, R. Easther, and L. C. Price, arXiv:1403.5922.
[9] A. Ashoorioon, K. Dimopoulos, M. M. Sheikh-Jabbari, and G. Shiu, arXiv:1403.6099.
[10] J. -Q. Xia, Y.-F. Cai, H. Li, and X. Zhang, Phys. Rev. Lett. **112**, 251301 (2014).
[11] M. Bastero-Gil, A. Berera, R. O. Ramos, and J. G. Rosa, arXiv:1404.4976.
[12] E. Giusarma, E. Di Valentino, M. Lattanzi, A. Melchiorri, and O. Mena, Phys. Rev. D **90**, 043507 (2014).
[13] J. -F. Zhang, Y.-H. Li, and X. Zhang, arXiv:1403.7028.
[14] C. Dvorkin, M. Wyman, D. H. Rudd, and W. Hu, arXiv:1403.8049.
[15] M. Archidiacono, N. Fornengo, S. Gariazzo, C. Giunti, S. Hannestad, and M. Laveder, J. Cosmol. Astropart. Phys. 06 (2014) 031.
[16] J. -F. Zhang, Y.-H. Li, and X. Zhang, Eur. Phys. J. C **74**, 2954 (2014).
[17] E. Di Valentino, E. Giusarma, M. Lattanzi, A. Melchiorri, and O. Mena, arXiv:1405.1860 [Phys. Rev. D (to be published)].
[18] M. Gerbino, A. Marchini, L. Pagano, L. Salvati, E. Di Valentino, and A. Melchiorri, Phys. Rev. D **90**, 047301 (2014).
[19] C. Cheng and Q.-G. Huang, arXiv:1403.5463.
[20] C. Cheng and Q.-G. Huang, arXiv:1405.0349.
[21] M. J. Mortonson and U. Seljak, arXiv:1405.5857.
[22] S. Dodelson, Phys. Rev. Lett. **112**, 191301 (2014).
[23] D. H. Lyth and A. R. Liddle, *The Primordial Density Perturbation: Cosmology, Inflation and the Origin of Structure* (Cambridge University Press, Cambridge, England, 2009), p. 497.
[24] A. A. Starobinsky, Phys. Lett. **91B**, 99 (1980).
[25] V. Mukhanov, Eur. Phys. J. C **73**, 2486 (2013).
[26] A. D. Linde, Phys. Lett. **129B**, 177 (1983).
[27] K. Freese, J. A. Frieman, and A. V. Olinto, Phys. Rev. Lett. **65**, 3233 (1990).
[28] F. C. Adams, J. R. Bond, K. Freese, J. A. Frieman, and A. V. Olinto, Phys. Rev. D **47**, 426 (1993).
[29] F. R. Bouchet *et al.* (COrE Collaboration), arXiv:1102.2181.
[30] A. Kogut, D. J. Fixsen, D. T. Chuss, J. Dotson, E. Dwek, M. Halpern, G. F. Hinshaw, S. M. Meyer *et al.*, J. Cosmol. Astropart. Phys. 07 (2011) 025.
[31] V. Mukhanov, *Physical Foundations of Cosmology* (Cambridge University Press, Cambridge, England, 2005), p. 421.
[32] A. Lewis, A. Challinor, and A. Lasenby, Astrophys. J. **538**, 473 (2000).
[33] A. Lewis and S. Bridle, Phys. Rev. D **66**, 103511 (2002).
[34] P. A. R. Ade *et al.* (Planck Collaboration), arXiv:1303.5062.
[35] P. A. R. Ade *et al.* (Planck Collaboration), arXiv:1303.5075.
[36] C. L. Bennett, D. Larson, J. L. Weiland, N. Jarosik, G. Hinshaw, N. Odegard, K. M. Smith, R. S. Hill *et al.*, Astrophys. J. Suppl. Ser. **208**, 20 (2013).
[37] F. L. Bezrukov and M. Shaposhnikov, Phys. Lett. B **659**, 703 (2008).
[38] F. Bezrukov, Classical Quantum Gravity **30**, 214001 (2013).
[39] S. Ferrara, A. Kehagias, and A. Riotto, Fortschr. Phys. **62**, 573 (2014).
[40] J. L. Cook, L. M. Krauss, A. J. Long, and S. Sabharwal, Phys. Rev. D **89**, 103525 (2014).
[41] K. Nakayama and F. Takahashi, Phys. Lett. B **734**, 96 (2014).
[42] P. Creminelli, D. López Nacir, M. Simonović, G. Trevisan, and M. Zaldarriaga, Phys. Rev. Lett. **112**, 241303 (2014).
[43] N. Okada, V. N. Şenoğuz, and Q. Shafi, arXiv:1403.6403.
[44] P. Di Bari, S. F. King, C. Luhn, A. Merle, and A. Schmidt-May, arXiv:1404.0009.
[45] N. Kaloper and A. Lawrence, Phys. Rev. D **90**, 023506 (2014).
[46] P. Creminelli, D. López Nacir, M. Simonović, G. Trevisan, and M. Zaldarriaga, arXiv:1405.6264.
[47] L. Dai, M. Kamionkowski, and J. Wang, Phys. Rev. Lett. **113**, 041302 (2014).
[48] T. Kobayashi and O. Seto, Phys. Rev. D **89**, 103524 (2014).
[49] K. Freese and W. H. Kinney, arXiv:1403.5277.
[50] K. Kohri, C. S. Lim, and C.-M. Lin, J. Cosmol. Astropart. Phys. 08 (2014) 001.
[51] L. Amendola *et al.* (Euclid Theory Working Group Collaboration), Living Rev. Relativity **16**, 6 (2013).